Self-consistent time-dependent harmonic approximation for the sine-Gordon model out of equilibrium

Yuri D. van Nieuwkerk and Fabian H. L. Essler
Rudolf Peierls Centre for Theoretical Physics, Parks Road, Oxford OX1 3PU
(Dated: August 1, 2019)

We derive a self-consistent time-dependent harmonic approximation for the quantum sine-Gordon model out of equilibrium and apply the method to the dynamics of tunnel-coupled one-dimensional Bose gases. We determine the time evolution of experimentally relevant observables and in particular derive results for the probability distribution of subsystem phase fluctuations. We investigate the regime of validity of the approximation by applying it to the simpler case of a nonlinear harmonic oscillator, for which numerically exact results are available. We complement our self-consistent harmonic approximation by exact results at the free fermion point of the sine-Gordon model.

I. INTRODUCTION

The study of isolated quantum many-body systems out of equilibrium has seen a series of striking successes in the past decades, characterized by a fruitful interplay between theory and experiment. The possibility of analyzing the non-equilibrium dynamics of one-dimensional gases in particular[1–3] stimulated a multitude of theoretical developments concerning the equilibration of observables and spreading of correlations and entanglement after quantum quenches[4–12]. In turn, cold atom experiments have been successful in confirming many of these theoretical ideas directly[13–18]. A particularly nice example is offered by matter-wave interferometry[19] using pairs of split one-dimensional Bose gases[15–17,20–25], which can often be modelled theoretically using Luttinger Liquid theory[26,27]. This approach permits a theoretical description of the dynamics of observables as well as their full quantum mechanical probability distribution functions[28–30], which were found to be in good correspondence with experiment[15,17].

Of particular interest to our work is the case when a pair of one-dimensional Bose gases is connected via a finite potential barrier[21–24], so that tunnelling can occur. The low-energy physics of this setup is governed by a quantum sine-Gordon model[31]

$$H_{\rm SG} = H_0 - J\int_L dx\cos\phi(x),$$
$$H_0 = \frac{v}{2\pi}\int_L dx\ \left[K(\partial_x\phi(x))^2 + \frac{1}{K}(\partial_x\theta(x))^2\right]. \tag{1}$$

Here the bosonic fields ϕ and $\partial_x\theta$ satisfy canonical commutation relations $[\partial_x\theta(x),\phi(y)] = i\pi\delta(x-y)$ and are compactified according to $\phi = \phi + 2\pi$ and $\theta = \theta + \pi$. The real parameters v, J and $K > 1/2$ are as yet undetermined, but will acquire physical meaning in what follows. Experiments have focussed on finite temperature equilibrium properties[32] and non-equilibrium dynamics in presence of a nonzero initial phase difference[33] in the large-K regime. The latter experiments observed damped phase oscillations and relaxation to a phase-locked state, for which no theoretical explanation is known[34]. On the theoretical side there have been a number of works investigating the dynamics after quantum quenches to the sine-Gordon model. The limit $K\to\infty$ is amenable to a simple harmonic approximation[36–39], while at $K = 1/4$ the sine-Gordon model is equivalent to a free massive Dirac fermion and this can be used to obtain exact results[36,37]. In Ref. 35 a combination of semiclassical and perturbative methods was used to study the rephasing dynamics for two coherently split condensates without initial phase difference. Ref. 40 investigated the time dependence of one-point functions in the repulsive regime $K < 1/4$ for quenches from an "integrable" initial state by a combination of quench action[41,42] and linked-cluster expansion[43,44] methods. In Ref. 45 semiclassical methods[46,47] were applied to the same problem, while quenches from the same class of initial states to the attractive regime of the sine-Gordon model were considered in Refs 48–50. A novel semiclassical approach was developed in Ref. 51 and used to determine the time-dependence of one and two-point functions as well as the probability distribution of the phase. The truncated conformal space approach[52] was applied in Ref. 53 to study the time evolution of two and four-point functions after a quantum quench. A very recent work[54] addressed the phase-locking behaviour observed in the experiments[33] by applying a combination of numerical methods to the phase dynamics in the sine-Gordon model. These findings are at variance with the experimental observations, although the parameter window of the methods does not currently extend to the relevant regime of weak interactions. This means that in spite of tentative evidence to the contrary, it is as yet unclear whether the observed relaxation to a phase-locked state is captured by a description in terms of a sine-Gordon model.

The aim of this work is to contribute to this discussion by improving on the known quadratic approximation, valid at weak interaction strengths, and replacing it by a self-consistent harmonic approximation which approximates the full cosine potential in a time-dependent manner. Such an approximation has been successfully employed for ϕ^4-theory,

both in equilibrium[55] and out of equilibrium[56], and it has been formulated for the sine-Gordon model in Ref. 57. We present an alternative derivation of the method, leading to a set of coupled nonlinear equations of motion, which we solve numerically. This not only yields correlation functions, but also allows for the calculation of full distribution functions for the relevant observables. As an application of this method, we show that for squeezed initial states relevant for cold-atom experiments, the model exhibits density-phase oscillations with a time-dependent modulation of the amplitude. This amplitude modulation depends on the number-squeezing factor which characterizes the initial state. These results are complemented by exact calculations at the free fermion point of the sine-Gordon model, where strong damping of density-phase oscillations is observed.

II. DERIVATION OF THE SELF-CONSISTENT HARMONIC APPROXIMATION

Our point of departure is the quantum sine-Gordon model (1) on a ring of circumference L. We are interested in non-equilibrium dynamics after a quantum quench: the system is prepared in an initial pure state $|\psi(0)\rangle$ which is not an eigenstate of $H_{\rm SG}$ and which satisfies Wick's theorem. The subsequent time evolution of the system is then described by the time-dependent Schrödinger equation

$$|\psi(t)\rangle = e^{-iH_{\rm SG}t}|\psi(0)\rangle \ . \tag{2}$$

The self-consistent time-dependent harmonic approximation (SCTDHA) consists of replacing the exact time evolution operator with

$$e^{-iH_{\rm SG}t} \longrightarrow U_{\rm SCH}(t) = Te^{-i\int_0^t H_{\rm SCH}(\tau)d\tau} \ , \tag{3}$$

where

$$H_{\rm SCH}(t) = H_0 - J\int_L dx\big[f(x,t) + g(x,t)\phi(x) + h(x,t)\phi^2(x)\big]. \tag{4}$$

The time-dependent functions in (4) are determined in a self-consistent way as follows. We assume that the Bose field can be decomposed into creation/annihilation parts with respect to the time evolved state $|\psi_{\rm SCH}(t)\rangle = U_{\rm SCH}(t)|\psi(0)\rangle$

$$\begin{aligned} \phi(x) &= \langle\phi(x)\rangle_t + \phi^+(x,t) + \phi^-(x,t) \ , \\ \phi^-(x,t)|\psi_{\rm SCH}(t)\rangle &= 0 = \langle\psi_{\rm SCH}(t)|\phi^+(x,t) \ , \end{aligned} \tag{5}$$

where the commutator $[\phi^+(x,t),\phi^-(y,t)]$ is a c-number and

$$\langle\phi(x)\rangle_t = \langle\psi_{\rm SCH}(t)|\phi(x)|\psi_{\rm SCH}(t)\rangle. \tag{6}$$

The existence of the decomposition (5) holds for the class of initial states described in Appendix A. We then define a *normal ordering* operation $:\phi^n:$ by stipulating that in a normal ordered expression all $\phi^-(t)$ appear on the rightmost side of any product. In particular we have

$$:\phi^n: := \sum_{m=0}^{n}\binom{n}{m}\langle\phi\rangle_t^{n-m} :\big(\phi^+(t)+\phi^-(t)\big)^m: . \tag{7}$$

Applying this normal ordering procedure to $\cos(\phi)$ we find

$$\cos\big(\phi(x)\big) = :\cos\big(\phi(x)\big): e^{-\frac{1}{2}\langle\langle\phi^2(x)\rangle\rangle_t} = \sum_{n=0}^{\infty}\frac{(-1)^n}{(2n)!}:\phi^{2n}(x): e^{-\frac{1}{2}\langle\langle\phi^2(x)\rangle\rangle_t}, \tag{8}$$

where $\langle\langle . \rangle\rangle$ denotes connected correlation functions

$$\langle\langle\phi^2(x)\rangle\rangle_t = \langle\phi^2(x)\rangle_t - \langle\phi(x)\rangle_t^2 . \tag{9}$$

We now use (7) and neglect all higher than quadratic terms in fluctuations i.e. we set

$$:\big(\phi^+(t)+\phi^-(t)\big)^m: \longrightarrow 0 \quad \forall \quad m>2. \tag{10}$$

This results in the time-dependent Hamiltonian (4) subject to the self-consistency conditions

$$\begin{aligned} f(x,t) &= \left[\Big(1+\frac{1}{2}\Big(\langle\langle\phi^2(x)\rangle\rangle_t - \langle\phi(x)\rangle_t^2\Big)\Big)\cos\big(\langle\phi(x)\rangle_t\big) + \langle\phi(x)\rangle_t \sin\big(\langle\phi(x)\rangle_t\big)\right] e^{-\frac{1}{2}\langle\langle\phi^2(x)\rangle\rangle_t} \ , \\ g(x,t) &= \left[\langle\phi(x)\rangle_t\cos\big(\langle\phi(x)\rangle_t\big) - \sin\big(\langle\phi(x)\rangle_t\big)\right] e^{-\frac{1}{2}\langle\langle\phi^2(x)\rangle\rangle_t} \ , \\ h(x,t) &= -\frac{1}{2}\cos\langle\phi(x)\rangle_t\, e^{-\frac{1}{2}\langle\langle\phi^2(x)\rangle\rangle_t}. \end{aligned} \tag{11}$$

A. Alternative Derivation

The SCTDHA is perhaps more naturally derived on the level of the equations of motion, as is done in Ref. 57. Since the cosine term in the sine-Gordon Hamiltonian (1) contains all positive, even powers of the field, it generates an infinite set of coupled partial differential equations relating the time evolution of all connected n-point functions, i.e. a BBGKY-hierarchy. This hierarchy is truncated by assuming that all connected n-point functions are negligible above a certain order n. In the SCTDHA, one truncates at quadratic order, meaning all higher cumulants are set to zero. For a Gaussian initial state there will always be some time scale up to which this is a good approximation, see e.g. Refs 58 and 59. Following Ref. 57 we separate the field into its expectation value and fluctuations around it

$$\phi(x,t) = \langle\phi(x,t)\rangle + \hat{\chi}(x,t). \tag{12}$$

The equation of motion of the Bose field is then

$$\begin{aligned}\left(v^2\partial_x^2 - \partial_t^2\right)\phi(x,t) &= \frac{v\pi J}{K}\sin\left(\phi(x,t)\right) \\ &= \frac{v\pi J}{K}\left[\sin\left(\langle\phi(x,t)\rangle\right)\cos\left(\hat{\chi}(x,t)\right) + \cos\left(\langle\phi(x,t)\rangle\right)\sin\left(\hat{\chi}(x,t)\right)\right] .\end{aligned} \tag{13}$$

Assuming that all higher cumulants of the fluctuation field are negligible the right-hand side can be approximated by

$$\frac{v\pi J}{K}\left[\sin\left(\langle\phi(x,t)\rangle\right) :\cos\left(\hat{\chi}(x,t)\right): + \cos\left(\langle\phi(x,t)\rangle\right) :\sin\left(\hat{\chi}(x,t)\right):\right] e^{-\frac{1}{2}\langle\langle\hat{\chi}^2\rangle\rangle}. \tag{14}$$

The equation of motion for the expectation value then becomes

$$\left(v^2\partial_x^2 - \partial_t^2\right)\langle\phi(x,t)\rangle = \frac{v\pi J}{K}\sin\left(\langle\phi(x,t)\rangle\right)e^{-\frac{1}{2}\langle\langle\hat{\chi}^2\rangle\rangle}. \tag{15}$$

Finally we linearize the equation of motion for the fluctuation field

$$\left[v^2\partial_x^2 - \partial_t^2 - \frac{v\pi J}{K}\cos\left(\langle\phi(x,t)\rangle\right)e^{-\frac{1}{2}\langle\langle\hat{\chi}^2(x,t)\rangle\rangle}\right]\hat{\chi}(x,t) = 0 . \tag{16}$$

It is easy to verify that the equations of motion (15) and (16) are exactly the same as the Heisenberg equations of motion with regards to $H_{\mathrm{SCH}}(t)$

$$\frac{\partial\phi(x,t)}{\partial t} = iU_{\mathrm{SCH}}(t)[H_{\mathrm{SCH}}(t),\phi(x)]U^\dagger_{\mathrm{SCH}}(t). \tag{17}$$

B. Mode expansion

The mode expansions for the Bose field and the dual field can be cast in the form

$$\phi(x) = \sum_j u_j e^{iq_jx}\left(b_j - b^\dagger_{-j}\right) , \tag{18}$$

$$\frac{\partial_x\theta(x)}{\pi} = \frac{-i}{2u_0L}\left(b_0 + b_0^\dagger\right) + \sum_{j\neq 0}\frac{ie^{iq_jx}}{2u_jL}\left(b_j + b^\dagger_{-j}\right) , \tag{19}$$

where $q_j = 2\pi j/L$ and we have introduced coefficients

$$u_j = \begin{cases}\left|\frac{\pi}{2q_jLK}\right|^{1/2}\mathrm{sgn}\left(q_j\right), & \text{if } j\neq 0 ,\\ \frac{i}{4}\sqrt{\frac{2v}{K}} & \text{if } j = 0 .\end{cases} \tag{20}$$

The zero momentum modes take account of the periodicity of the dual Bose field $\theta(x+L) = \theta(x) + \pi\delta N$, where δN is an operator with integer eigenvalues[26]. In (18,19) we have introduced creation/annihilation operators by

$$b_0 = -\left(i\sqrt{\frac{2K}{v}}\phi_0 + \frac{1}{2}\sqrt{\frac{v}{2K}}\delta N\right) , \tag{21}$$

where $[\delta N, \phi_0] = i$. The Bose field $\phi(x)$, though compactified with period 2π in the original sine-Gordon model, can not be compactified in the SCTDHA, since the harmonic approximation breaks the periodicity of the cosine potential. Instead, we take $\phi(x)$ and its zero mode ϕ_0 to have a spectrum ranging over all of $\mathbb{R}$. Local observables are not affected by this decompactification as long as we consider states where $\langle\phi(x)\rangle$ lies close to zero, and focus on regimes where $K \gg 1$, such that the variance of $\phi(x)$ is small.

By construction the free part of the Hamiltonian is diagonalized by the above mode expansions, as

$$H_0 = \frac{\pi v(\delta N)^2}{2KL} + \sum_{j\neq 0} v|q_j| b_j^\dagger b_j. \tag{22}$$

In order to describe time evolution in the self-consistent harmonic approximation it is convenient to carry out an initial state dependent canonical transformation.

C. Gaussian initial states

To guarantee the existence of a time scale over which the SCTDHA is accurate we prepare our system in a Gaussian initial state. In the following we restrict ourselves to translationally invariant Gaussian pure states for simplicity and refer to Ref. 60 for a discussion of the general case. In terms of the bosonic creation and annihilation operators any translationally invariant Gaussian pure state can be written in the form

$$|V, \vartheta, \varphi\rangle = \exp\left(V_0 \operatorname{sech}\vartheta_0 \, b_0^\dagger + \frac{1}{2}\sum_k e^{i\varphi_k} \tanh\vartheta_k \, b_k^\dagger b_{-k}^\dagger \right)|0\rangle \,, \tag{23}$$

where $\vartheta_k = \vartheta_{-k}$ and $\varphi_k = \varphi_{-k}$ are real coefficients. To simplify some of the equations below we introduce

$$V_k = \delta_{k,0} V_0 \in \mathbb{C} \,. \tag{24}$$

The operators

$$a_k = \cosh\vartheta_k \, b_k - e^{i\varphi_k} \sinh\vartheta_k \, b_{-k}^\dagger - V_k \,, \tag{25}$$

annihilate the initial state

$$a_k \, |V, \vartheta, \varphi\rangle = 0 \,. \tag{26}$$

The two sets of creation and annihilation operators are related by a canonical transformation

$$b_k = \cosh\vartheta_k \left[a_k + V_k\right] + e^{i\varphi_k} \sinh\vartheta_k \left[a_{-k}^\dagger + V_{-k}^\dagger\right]. \tag{27}$$

D. Equations of motion

The Hamiltonian $H_{\mathrm{SCH}}(t)$ has a mode expansion of the form

$$H_{\mathrm{SCH}}(t) = \sum_j \left[b_j^\dagger A_j(t) b_j + \frac{1}{2}\big(b_j B_j^*(t) b_{-j} + \text{h.c.}\big)\right] + D(t)\left(b_0 - b_0^\dagger\right) + C(t) \,, \tag{28}$$

where the coefficients $A_j(t), B_j(t)$ and $D(t)$ are functions of $g(t)$ and $h(t)$ via

$$\begin{aligned} A_j(t) &= v|p_j| - 2JL|u_j|^2 h(t) \,, \\ B_j(t) &= v|p_0|\delta_{j0} + 2JL|u_j|^2 h(t) \,, \\ D(t) &= -JLu_0 g(t) \,. \end{aligned} \tag{29}$$

In the above, we have defined $p_0 = 2\pi/vL$, and $C(t)$ is a real scalar which does not affect the equations of motion. The functions $g(t)$ and $h(t)$ are position independent as we have imposed periodic boundary conditions and assumed the initial state to be translationally invariant. The time evolution of b_j-operators is obtained from the Heisenberg equation of motion

$$i\frac{d}{dt} b_j(t) = U_{\mathrm{SCH}}(t) \left[b_j, H_{\mathrm{SCH}}(t)\right] U_{\mathrm{SCH}}^\dagger(t). \tag{30}$$

As $H_{\rm SCH}(t)$ couples only modes with either the same or equal but opposite index and in view of (27) the time evolved annihilation operators can be expressed as

$$b_j(t) = \delta_{j,0} R(t) + S_j(t) a_j + T_j^*(t) a_{-j}^\dagger \ . \tag{31}$$

The initial conditions follow from (27)

$$R(0) = V_0 \cosh\vartheta_0 + V_0^* e^{i\varphi_0} \sinh\vartheta_0 \ , \quad S_j(0) = \cosh\vartheta_j \ , \quad T_j^*(0) = e^{i\varphi_j} \sinh\vartheta_j \ . \tag{32}$$

The time dependence of $R(t), S_j(t)$ and $T_j(t)$ is obtained by substituting (31) in to (30), which gives a system of coupled, first order differential equations

$$\begin{aligned} i\dot{R}(t) &= A_0(t) R(t) + B_0(t) R^*(t) - D(t) \ , \\ i\dot{S}_j(t) &= A_j(t) S_j(t) + B_j(t) T_{-j}(t) \ , \\ -i\dot{T}_j(t) &= A_j^*(t) T_j(t) + B_j^*(t) S_{-j}(t). \end{aligned} \tag{33}$$

We stress that Eqns (33) are *non-linear* as A, B and D are functions of R, S and T by virtue of the self-consistency conditions (11). The time evolved Bose fields in our SCTDHA are given by

$$\phi(x,t) = -2|u_0| {\rm Im}\left(R(t)\right) + \sum_j u_j e^{iq_j x} \left(Q_j(t) a_j - Q_{-j}^*(t) a_{-j}^\dagger \right) \ , \tag{34}$$

where we have defined

$$Q_j(t) = S_j(t) - T_{-j}(t), \quad \bar{Q}_j(t) = S_j(t) + T_{-j}(t) \ . \tag{35}$$

Using that $a_j \left|V, \vartheta, \varphi\right\rangle = 0$ it is then straightforward to obtain equal-time correlation functions of the Bose field

$$\langle \phi(x,t) \rangle = -2|u_0| {\rm Im}\left(R(t)\right) \ , \tag{36}$$

$$\langle \phi(x,t)\phi(y,t) \rangle_{\rm conn} = \sum_j |u_j|^2 |Q_j(t)|^2 \cos\left(q_j\,(x-y)\right). \tag{37}$$

These expectation values determine the functions $g(t)$, $h(t)$ and by (29) the parameters $A_j(t)$, $B_j(t)$, $D_j(t)$. Substituting back into (33) we arrive at a closed system of differential equations for $R_j(t)$, $S_j(t)$ and $T_j(t)$. We solve this nonlinear system numerically to obtain the full time evolution of local operators in our SCTDHA.

E. Full distribution functions and multipoint correlation functions

A nice feature of the SCTDHA is that it makes it possible to analyze not only expectation values of local operators, but the full quantum mechanical probability distributions of observables on subsystems. This is of considerable experimental and theoretical interest[28,32,61–76]. An example relevant to realizations of the sine-Gordon model in split one-dimensional Bose gases are the probability distributions for the real and imaginary parts of the operator[28–30]

$$\hat{\mathcal{O}}_\ell = \int_{-\ell/2}^{\ell/2} dx \ e^{i\hat{\phi}(x)}. \tag{38}$$

It is convenient to define a joint probability distribution of the commuting operators ${\rm Re}(\hat{\mathcal{O}}_\ell)$ and ${\rm Im}(\hat{\mathcal{O}}_\ell)$

$$F_\ell(t,a,b) = \langle \psi_{\rm SCH}(t) | \delta\big({\rm Re}(\hat{\mathcal{O}}_\ell) - a\big) \delta\big({\rm Im}(\hat{\mathcal{O}}_\ell) - b\big) | \psi_{\rm SCH}(t) \rangle \ . \tag{39}$$

As shown in Appendix B it is possible to obtain a multiple integral representation for this quantity in the framework of the SCTDHA

$$\begin{aligned} F_\ell(t,a,b) = \int_{-\infty}^{\infty} \prod_j \left[d\alpha_j d\beta_j \frac{e^{-\frac{1}{2}|Q_j(t)|^{-2}\left(\alpha_j^2+\beta_j^2\right)}}{2\pi\,|Q_j(t)|^2} \right] \delta\left(a - \int_{-\ell/2}^{\ell/2} dx \cos\left(\Phi(x,t,\boldsymbol{\alpha},\boldsymbol{\beta})\right) \right) \\ \times\ \delta\left(b - \int_{-\ell/2}^{\ell/2} dx \sin\left(\Phi(x,t,\boldsymbol{\alpha},\boldsymbol{\beta})\right) \right) \ , \end{aligned} \tag{40}$$

where

$$\Phi(x,t,\boldsymbol{\alpha},\boldsymbol{\beta}) = \langle\phi(0,t)\rangle - \sum_j |u_j|\Big(\alpha_j \cos(p_j x) + \beta_j \sin(p_j x)\Big). \tag{41}$$

We see that the distribution function is determined by the expectation value $\langle\phi(0,t)\rangle$, set by $R(t)$ via (36), along with quadratic fluctuations α_j and β_j, determined by the covariance matrix $|Q_j(t)|^2$. The essential quantities $R(t)$ and $Q(t)$ are obtained by solving the nonlinear, self-consistent system of equations (33). The distribution function (40) can be conveniently sampled: one draws numbers α_j and β_j from a Gaussian distribution with covariance matrix $|Q_j(t)|^2$ and computes the corresponding values of $\int_{-\ell/2}^{\ell/2} dx \exp(i\Phi(x,t,\boldsymbol{\alpha},\boldsymbol{\beta}))$. Placing real and imaginary parts of these values in a two-dimensional histogram and normalizing the result yields $F_\ell(t,a,b)$. Examples of such distribution functions are presented in Section IV C. As a corollary of the derivation in Appendix B, we also obtain multi-point correlation functions of the vertex operator $e^{i\sigma\phi(x)}$, e.g.

$$\left\langle e^{i\sigma\phi(x,t)} e^{i\tau\phi(0,t)} \right\rangle = e^{i(\sigma+\tau)\langle\phi(0,t)\rangle} e^{-\frac{1}{2}\sum_j |u_j|^2 |Q_j(t)|^2 \left(\sigma^2+\tau^2+2\sigma\tau\cos(q_j x)\right)}. \tag{42}$$

III. SELF-CONSISTENT HARMONIC APPROXIMATION IN EQUILIBRIUM

If we choose self-consistent normal ordering with respect to the ground state rather than some time evolved initial state our approximation reduces to the usual self-consistent harmonic approximation for the sine-Gordon model[77]. In the linear response regime at zero temperature many exact results are available for the sine-Gordon model, see e.g. Ref. 78, and it is instructive to use these to benchmark the SCHA. The exact breather mass of the sine-Gordon model is[79]

$$\Delta_1 = 2\sin\left(\frac{\pi\chi}{2}\right)\frac{2}{\sqrt{\pi}}\frac{v}{\xi}\frac{\Gamma(\chi/2)}{\Gamma((1+\chi)/2)}\left[\frac{\pi}{2}\frac{\xi^2}{v}J\frac{\Gamma(\frac{1}{1+\chi})}{\Gamma(\frac{\chi}{1+\chi})}\right]^{(1+\chi)/2}, \tag{43}$$

where $\chi = 1/(8K-1)$ and the length scale ξ corresponds to a cutoff in momentum space at $k_c = 2\pi/\xi$.

Normal ordering with regards to the (self-consistent) ground state results in a time-independent Hamiltonian of the same structure as $H_{\rm SCH}(t)$ in (28) and (29)), but with time-independent parameters

$$g = 0\,, \qquad h = -\frac{1}{2}e^{-\frac{1}{2}\langle\phi^2\rangle}. \tag{44}$$

This Hamiltonian can be diagonalized by a Bogoliubov transformation of the b-operators

$$\begin{aligned} b_j &= \cosh(\gamma_j)c_j + \sinh(\gamma_j)c_{-j}^\dagger\,, \\ e^{-2\gamma_j} &= \frac{\pi}{2KL|u_j|^2}[(vq_j)^2+\Delta^2]^{-\frac{1}{2}}\,, \end{aligned} \tag{45}$$

where we have defined

$$\Delta^2 = -2h\frac{\pi v J}{K}. \tag{46}$$

In terms of the Bogoliubov bosons we have

$$H_{\rm SCH} = \sum_j \left[\sqrt{(vq_j)^2+\Delta^2}\, c_j^\dagger c_j\right] + \tilde{C}\,. \tag{47}$$

The ground state of $H_{\rm SCH}$ the vacuum state of the c-bosons $c_j|0\rangle = 0$. The self-consistency condition for h is then obtained by calculating $\langle\phi^2\rangle = \langle 0|\phi^2(x)|0\rangle$

$$\langle\phi^2\rangle = \frac{\pi v}{2KL}\sum_j \frac{1}{\sqrt{v^2q_j^2 + \frac{\pi v J}{K}e^{-\frac{1}{2}\langle\phi^2\rangle}}}. \tag{48}$$

A simple quadratic (*non* self-consistent) approximation of $H_{\rm SG}(t)$[38,39] would be given by $g=0$ and $h=-1/2$, so that

$$\Delta_{\rm qdr}^2 = \frac{\pi v J}{K}. \tag{49}$$

In Fig. 1, we present a comparison between the gap of the first breather in the sine-Gordon model (solid lines), the gap in the completely quadratic model (dotted lines) and the gap in the SCHA (dashed line). This is the appropriate comparison to make because in the K regime of interest the first breather has the smallest excitation gap over the ground state. For large enough values of K, both the SCHA and the fully quadratic model provide accurate approximations. For smaller values of K, however, the self-consistent approximation clearly offers a much better prediction of Δ than the simple harmonic approximation does. Close to the Luther-Emery point, which lies at $K = 1/4$ in our conventions, the predictions from the SCHA become poor as well.

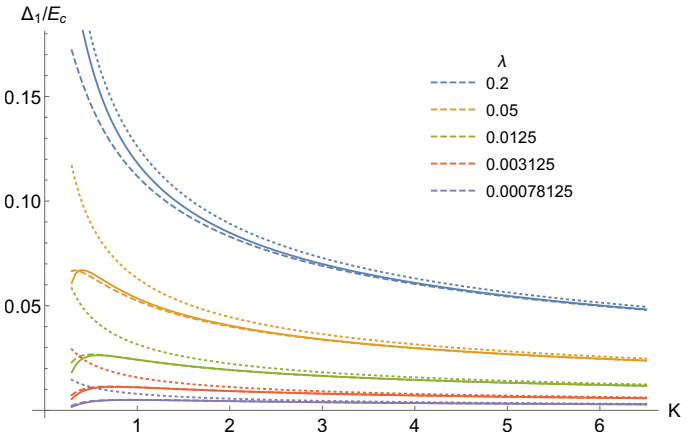

FIG. 1. Comparison between the mass gap for the fully quadratic model with $h = -1/2$ (dotted), the SCHA (dashed) and the exact result for the sine-Gordon Hamiltonian (solid curves), for several values of the dimensionless coupling $\lambda = \xi^2 J/v$. The gaps are plotted via their ratio with the cutoff energy scale, $E_c = 2\pi v/\xi$.

IV. REALIZATION BY TUNNEL-COUPLED BOSE GASES

A very interesting experimental realization of the sine-Gordon Hamiltonian (1) arises by tunnel-coupling a pair of one-dimensional Bose gases[31,32] $H = H_{\rm LL} + H_{\rm tunn}$ with

$$H_{\rm LL} = \sum_{j=1,2} \int dx \left[\frac{1}{2m} \partial_x \psi_j^\dagger \partial_x \psi_j + g\, \psi_j^\dagger \psi_j^\dagger \psi_j \psi_j \right] , \tag{50}$$

$$H_{\rm tunn} = -T_\perp \int dx \left(\psi_1^\dagger \psi_2 + \psi_2^\dagger \psi_1 \right) . \tag{51}$$

Here ψ_j are complex Bose fields with commutation relations $\left[\psi_i(x), \psi_j^\dagger(x')\right] = \delta_{i,j}\delta(x-x')$. At low energies the model (50), (51) can be bosonized using[26]

$$\psi_j \sim \sqrt{\rho_0 + \partial_x \theta_j(x)/\pi}\; e^{i\phi_j(x)} , \tag{52}$$

where ϕ_j are real Bose fields, θ_j the associated dual fields and ρ_0 the average density of bosons. Expressing the resulting Hamiltonian in terms of symmetric and antisymmetric combinations $\phi_{s,a} = \phi_1 \pm \phi_2$, $\theta_{s,a} = (\theta_1 \pm \theta_2)/2$ gives a decoupled theory of a free compact Boson and a sine-Gordon model

$$\mathcal{H} = \sum_{j=s,a} \frac{v}{2\pi} \int dx \left[K(\partial_x \phi_j(x))^2 + \frac{1}{K}(\partial_x \theta_j(x))^2 \right] - J \int dx\ \cos \hat{\phi}_a(x) . \tag{53}$$

The (less relevant) coupling between the two sectors will be analyzed in a forthcoming publication[60]. Importantly the symmetric sector only gives negligible contributions to the experimentally relevant observables in the large-K regime[73]. As the initial states of interest do not mix the two sectors and the observables of interest only involve ϕ_a it is possible to restrict the analysis to the sine-Gordon model describing the antisymmetric sector. To ease notation we drop the corresponding subscript in what follows.

The cutoff for the low-energy description (53) is given by the healing length of the gas $\xi = \pi/mv$ and we have defined $J = 2\rho_0 T_\perp$. For weak interactions, the effective parameters v and K can be related[31,80] to the parameters in

the microscopic model (50) by

$$v = \frac{\rho_0}{m}\sqrt{\gamma}\left(1-\frac{\sqrt{\gamma}}{2\pi}\right)^{1/2}, \quad K = \frac{\pi}{2\sqrt{\gamma}}\left(1-\frac{\sqrt{\gamma}}{2\pi}\right)^{-1/2}.$$

Here $\gamma = mg/\rho_0$ is the dimensionless interaction parameter. For later convenience we define a dimensionless coupling constant for the cosine term by

$$\lambda = \frac{\xi^2 J}{v}. \tag{54}$$

In the experiments by the Vienna group an initial state is prepared by splitting of a single one-dimensional condensate into two[33], which can be modelled by an initial condition[29,30]

$$\left\langle \frac{\partial_x\hat{\theta}(x)}{\pi}\frac{\partial_y\hat{\theta}(y)}{\pi}\right\rangle_c = \eta\frac{\rho}{2}\delta_\xi(x-y)\ . \tag{55}$$

Here δ_ξ denotes a delta function which is smeared over the healing length of the gas. In terms of the squeezed coherent state (23), this initial condition is obtained[30] by choosing Bogoliubov angles $\varphi_j = 0$ and

$$e^{-2\vartheta_j} = \begin{cases} \frac{|q_j|K}{\pi\eta\rho}\ , & \text{if } j\neq 0\ , \\ \frac{4K}{vL\eta\rho}\ , & \text{if } j = 0\ . \end{cases} \tag{56}$$

The parameter η tunes the number and phase fluctuations in the initial state.

A. Choice of parameters

In order to enable a comparison with experimental observations the parameters defining our model (53) should be fixed following Ref. 25: the one-dimensional density is taken to be $\rho_0 = 45\,\mu\text{m}^{-1}$, the healing length $\xi = \hbar\pi/mv = \pi\times 0.42\,\mu$m and longitudinal size $L = 160\,\xi$. Note that the latter is a factor 2 larger than the length reported in 25. We have made this adjustment to be able to follow the dynamics over longer timescales, before boundary effects come into play. For the case of ^{87}Rb atoms, the above amounts to $L\approx 212\,\mu$m, with a sound velocity given by $v\approx 1.738\cdot 10^{-3}\,$m/s and a Luttinger parameter of $K\approx 28$, in our conventions.

In order to explore the SCTDHA more generally we have also considered smaller values of the Luttinger parameter K. In Figs 2, 3, 4 and 9 we show results for $K = 1$, where the difference between the SCTDHA and the simple harmonic approximation is much larger. The free fermion results shown in Fig. 8 correspond to $K = 1/4$.

B. Time-evolution of the zero mode

As we have restricted our analysis to translationally invariant situations the zero momentum modes of the Bose fields play a key role. In the full Hamiltonian (28) the zero momentum modes are sensitive to the dynamics of the finite momentum modes by virtue of the self-consistency conditions. It is instructive to ignore such effects and consider the SCTDHA for a toy model that involves only the zero mode

$$H_{\text{J}} = \frac{\pi v}{2KL}\delta\hat{N}^2 - JL\cos\left(\hat{\phi}_0\right), \tag{57}$$

where $\left[\delta\hat{N},\hat{\phi}_0\right] = i$ and we have retained the various parameters from the full model. As (57) involves only a single degree of freedom it is straightforward to obtain exact results by numerically integrating the corresponding Schrödinger equation. This allows us to benchmark the SCTDHA. As initial state we choose a squeezed state $|\chi(0)\rangle$ with wave function in the ϕ-representation

$$\chi(\phi) = \left(\frac{1}{2\pi\sigma^2}\right)^{1/4} e^{-\frac{(\phi-\Phi_0)^2}{4\sigma^2}} e^{-i\delta N_0\phi}, \tag{58}$$

where $\sigma^2 = 1/(2\eta\rho L)$ and Φ_0, δN_0 are free parameters. In the SCTDHA the Hamiltonian (57) is replaced by

$$H'_{\text{J}} = \frac{\pi v}{2KL}\delta\hat{N}^2 - JL\left(f(t)+g(t)\hat{\phi}_0+h(t)\hat{\phi}_0^2\right). \tag{59}$$

The self-consistency conditions for f, g and h are obtained from (11) by replacing $\phi(x) \to \hat{\phi}_0$. For reference, we also consider time evolution with a simple harmonic Hamiltonian obtained from (57) by expanding the cosine to second order in $\hat{\phi}_0$

$$H_{\rm HO} = \frac{\pi v}{2KL}\delta\hat{N}^2 + \frac{JL}{2}\hat{\phi}_0^2, \tag{60}$$

The ground state wave function of $H_{\rm HO}$ is given by (58) with $\Phi_0 = 0 = \delta N_0$ and $\eta_0 \equiv \rho^{-1}\sqrt{JK/v\pi}$.

In Fig. 2 and Appendix C we compare time evolution under the Hamiltonians $H_{\rm J}$ (green line), $H_{\rm HO}$ (red, dotted line), and $H'_{\rm J}$ (blue line), with $\Phi_0 = 0.1$ and two choices of initial state $|\chi(0)\rangle$. We observe fast oscillations of $\langle\hat{\phi}_0\rangle \equiv \langle\chi(t)|\hat{\phi}_0|\chi(t)\rangle$ in time with a slowly varying envelope. This envelope shrinks (Fig. 2) or expands (Appendix C), depending on the initial values Φ_0 and δN_0. We observe that the amplitude modulation is more pronounced when η/η_0 is either large or small, which corresponds to initial states with either large phase or number fluctuations. Such states are sensitive to the anharmonicity of the cosine potential and their time evolution will exhibit larger deviations from that of a simple harmonic oscillator. We see that the SCTDHA is significantly better than the simple harmonic

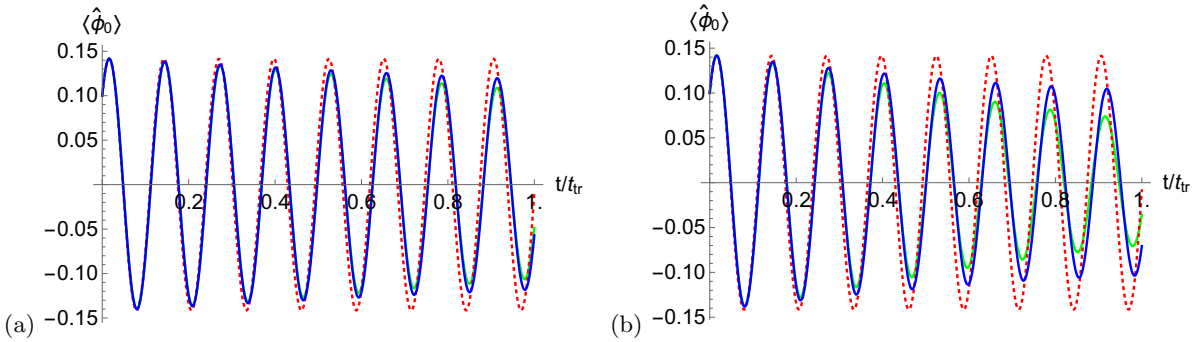

FIG. 2. Time-evolution of $\left\langle\hat{\phi}_0\right\rangle$ under the full Hamiltonian $H_{\rm J}$ (green line), the quadratic approximation $H_{\rm HO}$ (red dots) and the self-consistent harmonic approximation $H'_{\rm J}$ (blue line). The parameters are as described in section IV A and $\lambda = 0.12$, $K = 1$ and (a) $\eta = 4\eta_0$; (b) $\eta = 8\eta_0$. Times are displayed in units of the "traversal time" $t_{\rm tr} = L/(2v)$[7]. We have chosen the value $K = 1$ to highlight the differences between the three results, which are more pronounced for small K. Increasing the value of K leads to a better agreement between the three lines.

approximation $H_{\rm HO}$. The SCTDHA neglects higher connected correlations and is accurate as long as the latter are small. The contribution of the connected correlation functions to the expectation values of $\hat{\phi}_0^3$ and $\hat{\phi}_0^4$ are respectively

$$\left\langle\hat{\phi}_0^3\right\rangle = \left\langle\hat{\phi}_0^3\right\rangle_c + 3\left\langle\hat{\phi}_0^2\right\rangle_c\left\langle\hat{\phi}_0\right\rangle + \left\langle\hat{\phi}_0\right\rangle^3, \tag{61}$$

$$\left\langle\hat{\phi}_0^4\right\rangle = \left\langle\hat{\phi}_0^4\right\rangle_c + 4\left\langle\hat{\phi}_0^3\right\rangle_c\left\langle\hat{\phi}_0\right\rangle + 3\left\langle\hat{\phi}_0^2\right\rangle_c^2 + 6\left\langle\hat{\phi}_0^2\right\rangle_c\left\langle\hat{\phi}_0\right\rangle^2 + \left\langle\hat{\phi}_0\right\rangle^4. \tag{62}$$

Figs 3 and 4 show the time evolution of the neglected connected contributions and compare them to the full expectation value. By our choice of initial state the cumulants are initially zero and then grow in time. The growth of even

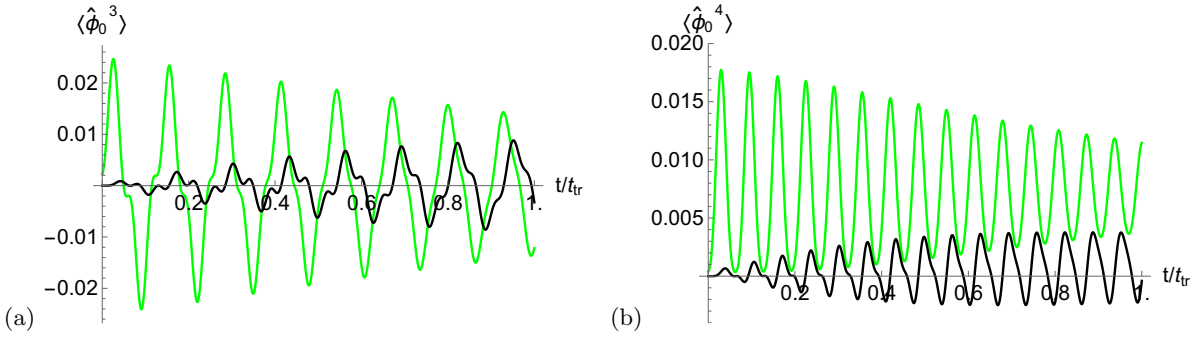

FIG. 3. Time-evolution of higher moments under the full cosine potential (green lines) compared to the contributions of the higher cumulants $\left\langle\hat{\phi}_0^3\right\rangle_c$ and $\left\langle\hat{\phi}_0^4\right\rangle_c$ (black lines). The parameters are as in Fig. 2(a).

cumulants is inhibited by choosing the squeezing parameter η close to η_0, whereas odd cumulants are inhibited by choosing Φ_0 and δN_0 close to 0. In our examples the cumulants remain small and concomitantly the SCTDHA is a good approximation.

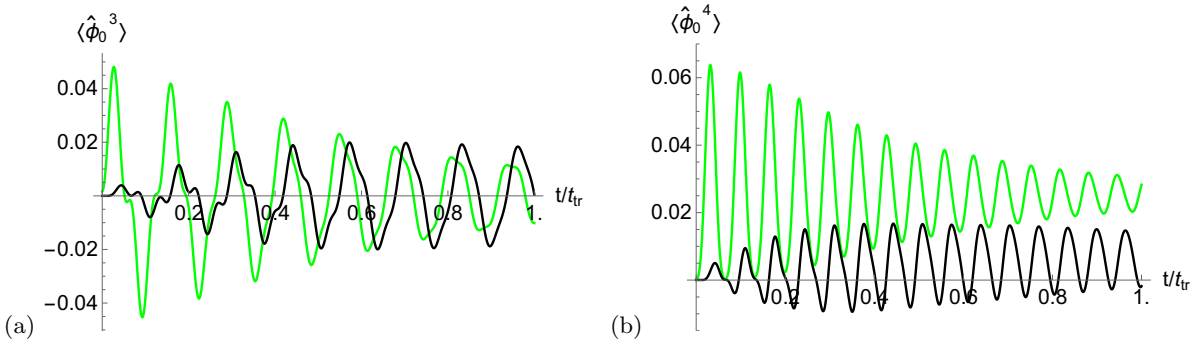

FIG. 4. The same as Fig. 3, but with squeezing parameter $\eta = 8\eta_0$.

C. Time-evolution in the SCTDHA for the sine-Gordon model

Having tested the self-consistent harmonic approximation in the controlled setting of single-body quantum mechanics, we now apply it to the sine-Gordon field theory, using the formalism developed in section II. Motivated by experiment we focus on the following observables:

- The one-point functions of density $\langle \partial_x \theta(x,t)\rangle/\pi$ and phase $\langle \phi(x,t)\rangle$. As we are restricting ourselves to translationally invariant situations these are x-independent.
- The full quantum mechanical probability distribution of $\int_{-\ell/2}^{\ell/2} dx\ \sin\big(\phi(x)\big)$

$$P_\ell(t,\mu) = \langle \psi_{\rm SCH}(t)|\delta\Big(\mu - \int_{-\ell/2}^{\ell/2} dx\ \sin\big(\phi(x)\big)\ \Big)|\psi_{\rm SCH}(t)\rangle\ . \tag{63}$$

In Fig. 5 we show parametric plots for the time dependence of the average density and phase in the SCTDHA for two different choices of parameters. In a purely harmonic theory the resulting trajectory would be closed, *cf.* the green line in Fig. 5(b). In contrast the amplitude of these oscillations gets modulated in time in the SCTDHA. We observe that these modulations become more pronounced as the squeezing parameter η is increased from its ground state value.

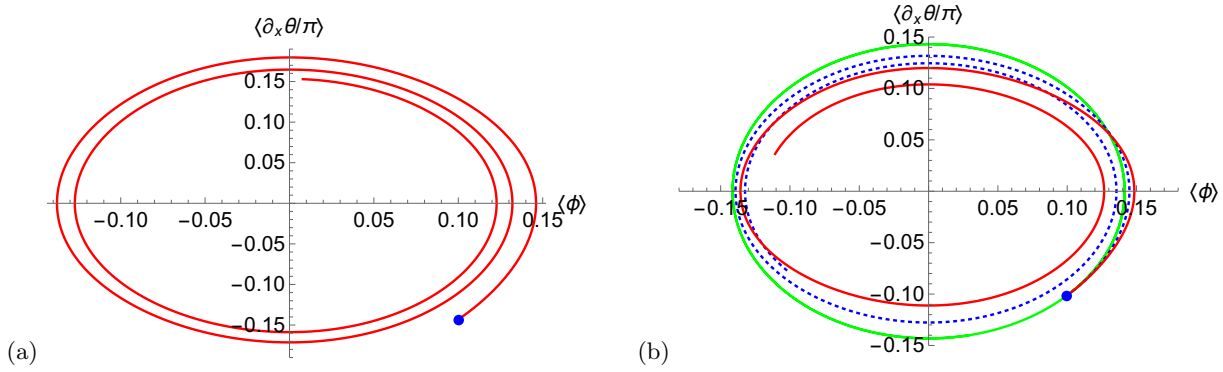

FIG. 5. (a) Density-phase oscillations in the SCTDHA. The parameters are as described in IV A and $K = 28, \lambda = 0.4, \eta = 1$. A modulation of the amplitude can be observed, which is not present in a simple quadratic approximation. (b) Same as (a) but with $\lambda = 0.2$, $\eta = 0.5$ (blue) and $\eta = 1$ (red). For comparison we also show the result of a simple harmonic approximation (green line). The modulation is seen to increase with η. In both panels, time runs until the traversal time $t_{\rm tr} = L/(2v)$.

We now turn to the probability distribution function $P_\ell(t,\mu)$. In recent experiments[33] it was observed that the variance of the probability distribution of the phase exhibits a rapid narrowing. A detailed explanation why these

experiments have access to the probability distribution of the phase itself is given in Ref. 73. An important question is whether such behaviour arises in the framework of the sine-Gordon model. In Figs 6 and 7 we show results for $P_\ell(t,\mu)$ for two integration lengths ℓ obtained in the SCTDHA and a simple harmonic approximation. Both display oscillatory behaviour in time and no narrowing of the variance is observed. In fact, the variance in the SCTDHA is slightly larger than the simple harmonic result. Comparing Fig. 6 to 7 we observe that increasing the integration length leads to a narrowing of $P_\ell(t,\mu)$.

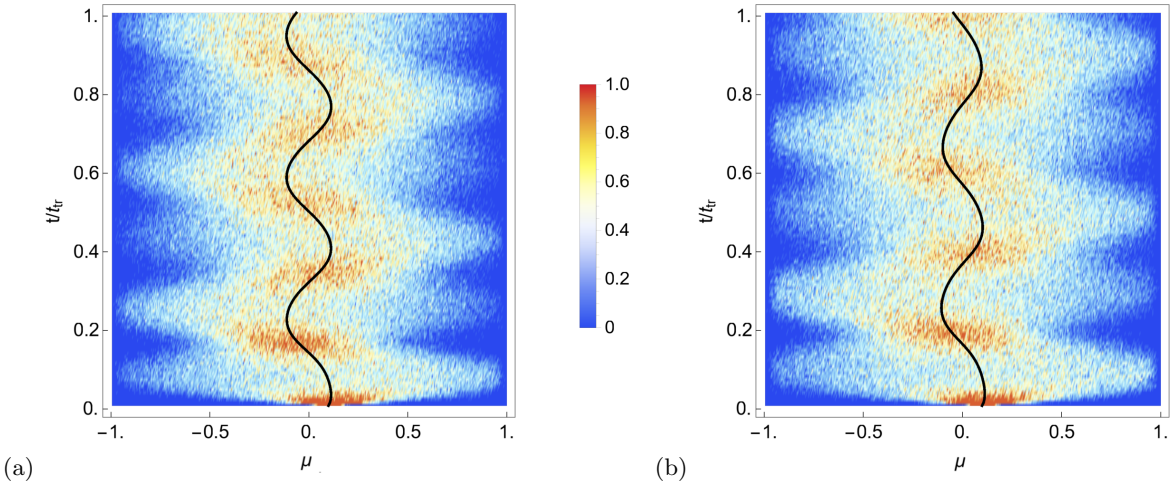

FIG. 6. (a) Probability distribution function $P_\ell(t,\mu)$ for a very short integration length $\ell = \xi$ in a simple harmonic approximation to the sine-Gordon model corresponding to $g = 0$ and $h = -1/2$ in (11). Parameters are as described in IV A with $K = 28$ and $\lambda = 0.2$. The black line shows the average of the PDF. (b) Same as (a) but computed in the SCTDHA.

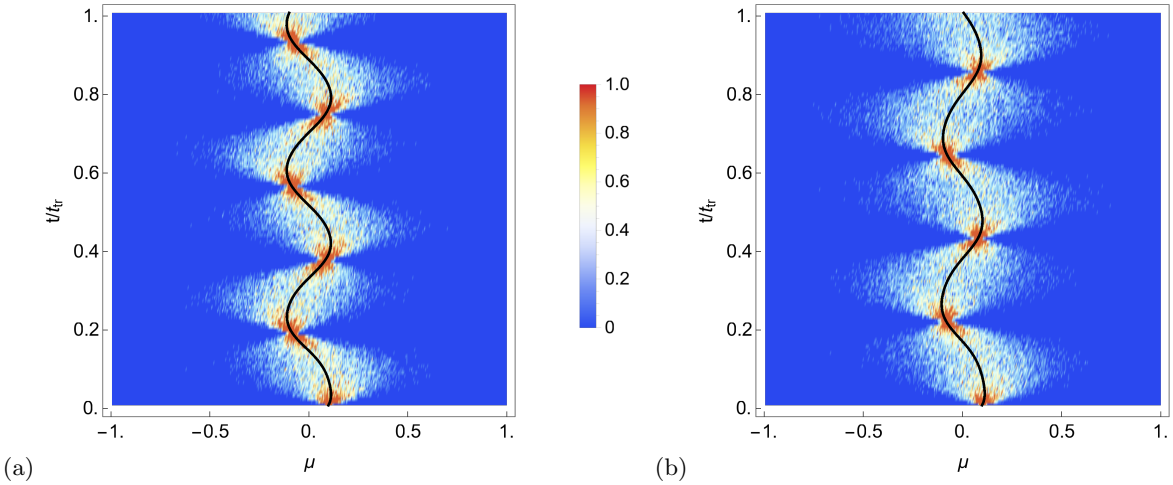

FIG. 7. Same as Fig. 6 but with a long integration length $\ell = L$.

V. DYNAMICS AT THE LUTHER-EMERY (LE) POINT

The SCTDHA is expected to work best at large values of the Luttinger parameter K. It is instructive to complement the large-K results presented above by exact results at the free fermion point of the sine-Gordon model. In our conventions the LE point occurs at $K = 1/4$. Quench dynamics at the LE point has been previously considered in Ref. 36 and 37 but that analysis did not cover the class of initial states of interest to us here. Two remarks are in order before we proceed:

- The LE point occurs at an unphysical value of K as far as the realization of the sine-Gordon model in the context of tunnel-coupled Bose gases is concerned. In that context the Luttinger parameter runs from $K = 1/2$ (hard-core repulsion) to $K \to \infty$ (non-interacting bosons).

- The SCTDHA is not expected to be a good approximation at the LE point. We have already seen an example of this in section III. The fundamental problem is that the relevant degrees of freedom at the LE point are solitons and antisolitons and these are not captured by a harmonic approximation. In light of this we will refrain from attempting to apply the SCTDHA to the sine-Gordon model at $K = 1/4$.

A. Mapping to free fermions

The sine-Gordon model can be fermionized using the bosonization identities

$$R(x) = \frac{F}{\sqrt{2\pi\xi}}\, e^{-i\sqrt{4\pi}\varphi_R(x)}, \quad L(x) = \frac{\bar{F}}{\sqrt{2\pi\xi}}\, e^{i\sqrt{4\pi}\varphi_L(x)}, \tag{64}$$

where $F = \sigma_x, \bar{F} = \sigma_y$ are Klein factors and $\varphi_{R/L}(x)$ are chiral Bose fields defined as

$$\varphi_{R/L} = \sqrt{\frac{K}{4\pi}}\phi \pm \frac{1}{\sqrt{4\pi K}}\,\theta\,. \tag{65}$$

The fields defined in (64) fulfil anticommutation relations $\{R^\dagger(x), R(y)\} = \{L^\dagger(x), L(y)\} = \delta(x-y)$. Expectation values are always taken with respect to the vector $(1,0)$ in Klein space. At the LE point the sine-Gordon Hamiltonian (1) is equivalent to

$$H_{\rm F} = \int_L dx\, \left[iv\left(L^\dagger(x)\partial_x L(x) - R^\dagger(x)\partial_x R(x)\right) + i\mu\left(R^\dagger(x)L(x) - L^\dagger(x)R(x)\right)\right], \tag{66}$$

where $\mu = \pi\xi J = \pi v\lambda/\xi$ and v, ξ and λ respectively are the physical sound velocity, coherence length and dimensionless coupling defined in section IV.

B. Time-evolution of density and phase

Our aim is to determine the expectation values of

$$\begin{aligned} \sin\left(\phi(x,t)\right) &= -\pi\xi\left[R^\dagger(x,t)L(x,t) + \text{h.c.}\right], \\ \frac{\partial_x\theta(x,t)}{\pi} - \frac{\langle\partial_x\theta(x,0)\rangle}{\pi} &= \frac{1}{2}\left[:L^\dagger(x,t)L(x,t): - :R^\dagger(x,t)R(x,t):\right]. \end{aligned} \tag{67}$$

Here products of operators at the same point are defined by means of a point-splitting prescription

$$:L^\dagger(x)L(x): \equiv \lim_{\epsilon\to 0}\left[L^\dagger(x-\epsilon)L(x+\epsilon) - \left\langle L^\dagger(x-\epsilon)L(x+\epsilon)\right\rangle_0\right], \tag{68}$$

where $\langle\ldots\rangle_0$ denotes the expectation value with respect to the initial state under consideration. In order to make some contact with our previous discussion we choose the initial state to be $|V,\varphi,\vartheta\rangle$ in (23) and (56), i.e.

$$\langle\mathcal{O}\rangle_0 \equiv \langle V,\varphi,\vartheta|\,\mathcal{O}\,|V,\varphi,\vartheta\rangle\,. \tag{69}$$

This state is translationally invariant, as is the Hamiltonian (66), so that the expectation values of the fields (67) do not depend on x for any t. To determine the time evolution of these expectation values, it is useful to define the following linear combinations of two-point functions,

$$\begin{aligned} D_\phi(x,t) &\equiv \left\langle R^\dagger(x)L(0)\right\rangle_t + \left\langle L^\dagger(x)R(0)\right\rangle_t + \left\langle R^\dagger(0)L(x)\right\rangle_t + \left\langle L^\dagger(0)R(x)\right\rangle_t, \\ D_\theta(x,t) &\equiv \left\langle L^\dagger(x)L(0)\right\rangle_t + \left\langle L^\dagger(0)L(x)\right\rangle_t - \left\langle R^\dagger(x)R(0)\right\rangle_t - \left\langle R^\dagger(x)R(0)\right\rangle_t, \end{aligned} \tag{70}$$

which only depend on t and the coordinate difference x due to translational invariance. The time evolution of these functions is governed by the pair of PDE's

$$\left(\partial_t^2 - 4v^2\partial_x^2 + 4\mu^2\right) D_\phi(x,t) = 0\,, \tag{71}$$

$$\partial_t D_\theta(x,t) + 2\mu D_\phi(x,t) = 0\,, \tag{72}$$

with initial conditions (69) and

$$\partial_t D_\phi(x,0) = 2\mu D_\theta(x,0) - 2v\partial_x\left[\left\langle R^\dagger(x)L(0)\right\rangle_0 + \left\langle R^\dagger(0)L(x)\right\rangle_0 - \left\langle L^\dagger(x)R(0)\right\rangle_0 - \left\langle L^\dagger(0)R(x)\right\rangle_0\right]. \tag{73}$$

These follow directly from the Heisenberg equation of motion (30) with Hamiltonian (66), combined with the translational invariance of the initial state $|V,\varphi,\vartheta\rangle$. The resulting solutions give access to the expectation values of the fields (67), via

$$\begin{aligned}\left\langle \sin\left(\phi(0,t)\right)\right\rangle &= -\frac{\pi\xi}{2} D_\phi(0,t),\\ \frac{\langle \partial_x\theta(0,t)\rangle}{\pi} - \frac{\langle \partial_x\theta(0,0)\rangle}{\pi} &= \frac{1}{4}\left[D_\theta(0,t) - D_\theta(0,0)\right].\end{aligned} \tag{74}$$

The rationale for considering the particular linear combinations of two-point functions (70) is to ensure cut-off independence: the initial two-point functions $\left\langle L^\dagger(x)L(0)\right\rangle_0$ and $\left\langle R^\dagger(x)R(0)\right\rangle_0$ diverge as $x\to 0$ in a way that depends on the UV cutoff. This cutoff-dependence enters the equations of motion of two-point functions via the short-distance behaviour of $D_\theta(x,0)$ in the initial condition (73). To eliminate this dependence we restrict ourselves to initial states $|V,\varphi,\vartheta\rangle$ for which $\langle \delta N\rangle_0 = 0$. For such states we have

$$\left\langle L^\dagger(0)L(x)\right\rangle_0 = -\left\langle L^\dagger(x)L(0)\right\rangle_0, \qquad \left\langle R^\dagger(0)R(x)\right\rangle_0 = -\left\langle R^\dagger(x)R(0)\right\rangle_0, \tag{75}$$

which implies that $D_\theta(x,0) = 0$ and renders the initial condition (73), and hence $D_\phi(x,t)$ and $D_\theta(x,t)$, cutoff-independent. In Fig. 8(a) we present results obtained by numerically integrating the system of PDEs for parameters as in IV A with $K = 1/4$. In contrast to the modest amplitude modulations encountered for larger K in Section IV C a strong damping of the density-phase oscillation is observed. The origin of the damping is simple dephasing.

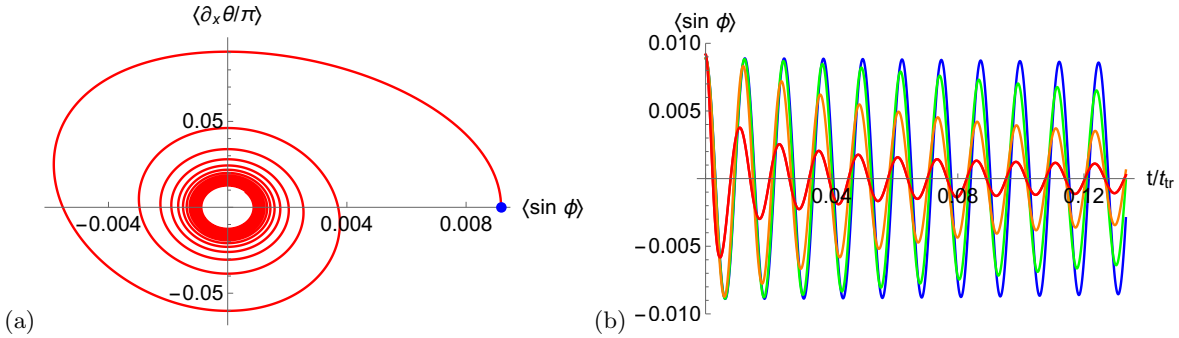

FIG. 8. (a) Strongly damped density-phase oscillation at the Luther-Emery point. Apart from taking $K = 1/4$, we have used the parameters as reported in (IV A), with the dimensionless coupling constant (54) set to $\lambda = 4$. The initial conditions are obtained from Eqs. (23) and (56) using the bosonization identity (64), with $\langle \delta N\rangle = 0$ and $\langle \phi_0\rangle = 0.1$ at $t = 0$. Due to the enhanced phase fluctuations at the Luther-Emery point for the state under consideration, the expectation value of the sine is reduced to $\langle \sin\phi\rangle \approx 0.009$, at $t = 0$. Time runs until the traversal time $t_{\rm tr} = L/(2v)$. (b) Oscillations of $\langle \sin\phi(0,t)\rangle$ for a range of initial states. Along with the initial conditions from (a) shown in red, we plot results where $D_\phi(x,0)$ is a Gaussian with standard deviation $\ell = \nu\xi$, for $\nu = 1$ (orange), $\nu = 2$ (green) and $\nu = 4$ (blue). For comparison, the initial conditions for $D_\phi(x,0)$ pertaining to the red line are sharply peaked around $x = 0$ with standard deviation $\ell \approx 0.34\xi$.

To shed some more light on the time-dependence of the observed dephasing behaviour we have considered other initial states. In Fig. 8(b) we compare the time evolution of $\langle \sin\phi(0,t)\rangle$ shown in Fig. 8(a) to that corresponding to initial states characterized by initial conditions

$$D_\phi(x,0) = -\frac{2}{\pi\xi}\left\langle \sin\phi(0,0)\right\rangle e^{-x^2/2(\nu\xi)^2}, \quad \nu = 1,2,4. \tag{76}$$

As the length scale $\ell = \nu\xi$ set by $D_\phi(x,0)$ is increased, the dephasing is seen to disappear. This can be understood by noting that (71) is simply a Klein-Gordon equation with dispersion relation $\omega_k = 2v\sqrt{k^2 + (\pi\lambda/\xi)^2}$. A wave packet $D_\phi(x,0)$ of initial width ℓ that is initially localized around the origin will disperse. The quantity of interest, $\langle \sin\phi(0,t)\rangle$, corresponds to the magnitude of $D_\phi(0,t)$, i.e. the part of the wave packet that remains at the origin. If the initial width of $D_\phi(x,0)$ is much smaller than the inverse gap, $\ell \ll \xi/(\pi\lambda)$, the initial time evolution will be dominated by the large-k Fourier modes where the dispersion is approximately linear. This causes the wave packet to essentially separate into parts that propagate ballistically with velocities $\pm 2v$. This leaves only a small weight near the origin and leads to a rapid decrease of $\langle \sin\phi(0,t)\rangle$. In contrast, the short-time evolution of wave packets with widths that far exceed the inverse gap $\ell \gg \xi/(\pi\lambda)$ is dominated by Fourier modes at small k, where the group velocity $\frac{\partial\omega}{\partial k} \ll v$ becomes very small. This results in a very slow evolution so that the weight at $x = 0$ is not substantially reduced for long times. The behaviour shown in Fig. 8(b) is in complete agreement with these expectations.

The above observations are quantified by going over to momentum space

$$R(x) = \frac{1}{\sqrt{L}} \sum_k e^{ikx}\ a_k\ , \quad L(x) = \frac{1}{\sqrt{L}} \sum_k e^{ikx}\ b_k\ . \tag{77}$$

The Hamiltonian is expressed in terms of the modes as

$$H = \sum_k \left(vk \left[a_k^\dagger a_k - b_k^\dagger b_k \right] + i\mu \left[a_k^\dagger b_k - b_k^\dagger a_k \right] \right). \tag{78}$$

The solution to the equations of motion are

$$\begin{pmatrix} a_k(t) \\ b_k(t) \end{pmatrix} = \begin{pmatrix} \cos(\omega_k t) - i \sin(\omega_k t) \cos(2\gamma_k) & \sin(\omega_k t) \sin(2\gamma_k) \\ -\sin(\omega_k t) \sin(2\gamma_k) & \cos(\omega_k t) + i \sin(\omega_k t) \cos(2\gamma_k) \end{pmatrix} \begin{pmatrix} a_k \\ b_k \end{pmatrix}, \tag{79}$$

where

$$\sin(2\gamma_k) = \frac{\mu}{\omega_k}\ , \quad \cos(2\gamma_k) = \frac{vk}{\omega_k}\ , \quad \omega_k = \mathrm{sgn}(k)\sqrt{(vk)^2 + \mu^2}. \tag{80}$$

Two-point functions of Fermi fields can be straightforwardly calculated. Using the bosonization identities (65), (64) they can then be related to expectation values of fields in the sine-Gordon model. Specializing to translationally invariant initial states with initial condition $\langle \partial_x \theta(x) \rangle_0 = 0$ we find

$$\begin{aligned} \frac{1}{\pi} \langle \partial_x \theta(x,t) \rangle_0 &= -\frac{1}{L} \sum_k \frac{\mu}{\omega_k} \sin(2\omega_k t)\ \mathrm{Re}\, \langle a_k^\dagger b_k \rangle\, , \\ \langle \sin \phi(x,t) \rangle_0 &= -\frac{1}{L} \sum_k 2\pi\xi \cos(2\omega_k t)\ \mathrm{Re}\, \langle a_k^\dagger b_k \rangle\, . \end{aligned} \tag{81}$$

The form of Eq. (81) allows us to relate the origin of the observed dephasing to properties of the initial state. If the weights $|\, \langle a_k^\dagger b_k \rangle\, |$ are concentrated in the small momentum region one can approximate

$$\langle \sin \phi(x,t) \rangle_0 \approx -\frac{\cos(2\mu t)}{L} \sum_k 2\pi\xi\ \mathrm{Re}\, \langle a_k^\dagger b_k \rangle\, , \tag{82}$$

showing undamped oscillations at frequency 2μ over a large time-window. On the other hand, if the weights are concentrated at large momenta strong dephasing sets in immediately.

VI. CONCLUSIONS

We have implemented a self-consistent time-dependent approximation for the quantum sine-Gordon model out of equilibrium. The approximation incorporates anharmonic effects of the cosine potential in a time-dependent manner by reducing higher-order fluctuations of the phase field to time-dependent mean field coefficients in the Hamiltonian. This leads to a time-dependent non-interacting Hamiltonian that can be analyzed by standard methods. Its simple structure allows for the calculation of multi-point correlation functions and full quantum mechanical probability distribution functions of some observables out of equilibrium.

As an application, we have considered tunnel-coupled, coherently split Bose-gases with an initial density- and phase offset. We found that expectation values of the density and phase exhibit oscillatory behaviour with amplitudes that are modulated in time. Such modulations are not observed in a simple harmonic approximation and arise from the anharmonicity of the cosine potential. These findings are of interest in relation to recent experiments by the Vienna group[33], where qualitatively similar behaviour was observed. However, the SCTDHA does not provide a quantitative explanation of the experimental findings. Moreover, the experiments show a rapid narrowing of the probability distribution of the phase, in contrast to what we find in the SCTDHA. Our results are in accord with recent numerical studies[54] and suggest that a simple sine-Gordon model is insufficient for describing the experiments.

Interestingly, an exact calculation at the free fermion point of the sine-Gordon model shows strong damping of oscillations, rather than the modest modulations encountered for weak interactions. While this is not applicable to experiments on tunnel-coupled bosons since the Luther-Emery point occurs at an unphysical value of the Luttinger parameter, it suggests that stronger interactions in the sine-Gordon model lead to an enhancement of the damping effects.

Our self-consistent method is very general and can in particular be applied to inhomogeneous situations. In a forthcoming publication we use it to analyze interactions between the symmetric and antisymmetric sectors in tunnel-coupled Bose gases and consider situations that are not translationally invariant[60]. The question whether such extensions of the theory lead to a better match with experiment will also be addressed there.

ACKNOWLEDGMENTS

We are grateful to Jörg Schmiedmayer and Marine Pigneur for stimulating discussions and to the Erwin Schrödinger International Institute for Mathematics and Physics for hospitality and support during the programme on *Quantum Paths*. This work was supported by the EPSRC under grant EP/N01930X and YDvN is supportedby the Merton College Buckee Scholarship and the VSB and Muller Foundations.

Appendix A: Initial states

In this Appendix we construct a class of initial states in which a Wick's theorem holds. Let b_j be the annihilation operators in the mode expansion of the Bose field and consider canonical transformations of the form

$$b_j = A_{jk}a_k + B_{kj}a_k^\dagger + v_j \ , \tag{A1}$$

where $[a_k, a_k^\dagger] = \delta_{j,k}$ and

$$a_j|i\rangle = 0. \tag{A2}$$

For the transformation to be canonical we require

$$AB = (AB)^T \ , \quad AA^\dagger - (B^\dagger B)^T = \mathbf{1}. \tag{A3}$$

By construction we have a Wick's theorem in the state $|i\rangle$ and the relevant one and two-point functions are

$$\begin{aligned} \langle i|b_j|i\rangle &= v_j \ , \\ \langle i|b_k b_p|i\rangle - \langle i|b_k|i\rangle\langle i|b_p|i\rangle &= (AB)_{kp} \ , \\ \langle i|b_k b_p^\dagger|i\rangle - \langle i|b_k|i\rangle\langle i|b_p^\dagger|i\rangle &= (AA^\dagger)_{kp}. \end{aligned} \tag{A4}$$

Appendix B: Joint Distribution Functions for the phase operator

The goal of this Appendix is to compute full distribution functions for the real and imaginary parts of the following operator

$$\hat{\mathcal{O}}_\ell = \int_{-\ell/2}^{\ell/2} dx e^{i\hat{\phi}(x,t)}, \tag{B1}$$

where the time evolution is calculated in the SCTDHA. The real and imaginary parts of $\hat{\mathcal{O}}_\ell$ are Hermitian and their respective measurement outcomes can be described by a joint PDF $F_\ell(t,a,b)$, which gives the probability density of simultaneously measuring the eigenvalue a for $\mathrm{Re}(\hat{\mathcal{O}}_\ell)$ and the eigenvalue b for $\mathrm{Im}(\hat{\mathcal{O}}_\ell)$ at time t. Once the joint PDF is known, expectation values of analytic functions $g(\mathrm{Re}(\hat{\mathcal{O}}_l), \mathrm{Im}(\hat{\mathcal{O}}_l))$ can be computed via

$$\left\langle g\left(\mathrm{Re}(\hat{\mathcal{O}}_\ell), \mathrm{Im}(\hat{\mathcal{O}}_\ell)\right)\right\rangle_t = \iint da\, db\, F_\ell(t,a,b) g(a,b). \tag{B2}$$

Expanding the approach of Ref. 30, this Appendix presents a computation of the PDF $F_\ell(t,a,b)$, by determining the generic $(m,n)^{\text{th}}$ moment $\langle (\mathrm{Re}(\mathcal{O}_\ell))^m (\mathrm{Im}(\mathcal{O}_\ell))^n\rangle$, and comparing it to the definition

$$M_{mn}(\ell,t) = \left\langle \left(\mathrm{Re}(\hat{\mathcal{O}}_\ell)\right)^m \left(\mathrm{Im}(\hat{\mathcal{O}}_\ell)\right)^n \right\rangle_t = \iint da\, db\, F_\ell(t,a,b) a^m b^n, \tag{B3}$$

from which $F_\ell(t,a,b)$ is then extracted. Expanding sines and cosines in terms of complex exponentials we have

$$M_{mn}(\ell,t) = \left(\frac{1}{2}\right)^m \left(\frac{1}{2i}\right)^n \sum_{\{s_j=\pm 1\}} \left(\prod_{j=m+1}^{m+n} s_j\right) \left(\prod_{k=1}^{m+n} \int_{-l/2}^{l/2} dx_k\right) \left\langle \prod_{l=1}^{m+n} e^{i s_l \phi_a(x_l,t)} \right\rangle. \tag{B4}$$

We recall that the mode expansion (34) for the time evolved Bose field has the form

$$\phi(x,t) = \langle\phi(0,t)\rangle + \sum_j u_j e^{iq_j x}\left(Q_j(t)a_j - Q_{-j}^*(t)a_{-j}^\dagger\right) \ , \tag{B5}$$

where a_j annihilate the initial state and with $\langle\phi(0,t)\rangle$ given by (36). To proceed we define functions

$$w_k(\boldsymbol{x}) = \sum_{j=1}^{m+n} s_j u_k e^{iq_k x_j}. \tag{B6}$$

The expectation value (B4) in the initial state can be expressed in the form

$$\left\langle \prod_{j=1}^{m+n} e^{is_j\phi_a(x_j,t)} \right\rangle = e^{i\sum_{j=1} s_j\langle\phi(0,t)\rangle} \left\langle e^{i\sum_j w_j(\boldsymbol{x})\left(Q_j(t)a_j - Q^*_{-j}(t)a^\dagger_{-j}\right)} \right\rangle \tag{B7}$$

$$= e^{i\sum_{j=1} s_j\langle\phi(0,t)\rangle} e^{-\frac{1}{2}\sum_j w_j(\boldsymbol{x})w_j^*(\boldsymbol{x})|Q_j(t)|^2}. \tag{B8}$$

The first exponent on the right-hand side of (B8) contains products of expressions involving different coordinates x_i and x_j with $i \neq j$. This means that the integrals in (B4) over the coordinates x_j cannot be separately carried out. We therefore perform a Hubbard-Stratonovich transformation based on the identity

$$e^{-\frac{q}{2}u^2} = \frac{1}{\sqrt{2\pi q}} \int dz e^{-\frac{1}{2q}z^2} e^{-iuz}. \tag{B9}$$

This gives

$$e^{-\frac{1}{2}\sum_j w_j(\boldsymbol{x})w_j^*(\boldsymbol{x})|Q_j(t)|^2} = \int_{-\infty}^{\infty} d\alpha_j \int_{-\infty}^{\infty} d\beta_j \frac{e^{-\frac{1}{2}|Q_j(t)|^{-2}\left(\alpha_j^2+\beta_j^2\right)}}{2\pi\,|Q_j(t)|^2} e^{-i\alpha_j \mathrm{Re}w_j(\boldsymbol{x}) - i\beta_j \mathrm{Im}w_j(\boldsymbol{x})}. \tag{B10}$$

Substituting (B8), (B10) into (B4), we obtain

$$\begin{aligned} M_{mn}(\ell,t) = \left(\frac{1}{2}\right)^m \left(\frac{1}{2i}\right)^n \sum_{\{s_l\}} \left(\prod_{l=m+1}^{m+n} s_l\right) \int_{-\infty}^{\infty} d\boldsymbol{\alpha} d\boldsymbol{\beta} \int_{-\ell/2}^{\ell/2} d\boldsymbol{x} \prod_j \frac{e^{-\frac{1}{2}|Q_j(t)|^{-2}\left(\alpha_j^2+\beta_j^2\right)} e^{is_j\langle\phi(0,t)\rangle}}{2\pi\,|Q_j(t)|^2} \\ \times \exp\left(-i\sum_k \left(\alpha_k \mathrm{Re}w_k(\boldsymbol{x}) + \beta_k \mathrm{Im}w_k(\boldsymbol{x})\right)\right). \end{aligned} \tag{B11}$$

Reinserting the vector $w_k(\boldsymbol{x})$ from Eq. (B6) and bringing the sum over signs s_l within the product, this simplifies to

$$\begin{aligned} M_{mn}(\ell,t) = \int_{-\infty}^{\infty} d\boldsymbol{\alpha} d\boldsymbol{\beta} \prod_j \frac{e^{-\frac{1}{2}|Q_j(t)|^{-2}\left(\alpha_j^2+\beta_j^2\right)}}{2\pi\,|Q_j(t)|^2} \\ \times \left(\int_{-\ell/2}^{\ell/2} dx \cos\left(\Phi(x,t,\boldsymbol{\alpha},\boldsymbol{\beta})\right)\right)^m \left(\int_{-\ell/2}^{\ell/2} dx \sin\left(\Phi(x,t,\boldsymbol{\alpha},\boldsymbol{\beta})\right)\right)^n, \end{aligned} \tag{B12}$$

where we have defined

$$\Phi(x,t,\boldsymbol{\alpha},\boldsymbol{\beta}) = \langle\phi(0,t)\rangle - \sum_j |u_j| \Big(\alpha_j \cos(p_j x) + \beta_j \sin(p_j x)\Big). \tag{B13}$$

Comparing (B12) to the definition of the joint PDF in (B3) gives the desired expression for the joint PDF

$$F_\ell(t,a,b) = \int_{-\infty}^{\infty} d\boldsymbol{\alpha} d\boldsymbol{\beta} \prod_j \frac{e^{-\frac{1}{2}|Q_j(t)|^{-2}\left(\alpha_j^2+\beta_j^2\right)}}{2\pi\,|Q_j(t)|^2} \tag{B14}$$

$$\times \quad \delta\left(a - \int_{-\ell/2}^{\ell/2} dx \cos\left(\Phi(x,t,\boldsymbol{\alpha},\boldsymbol{\beta})\right)\right) \delta\left(b - \int_{-\ell/2}^{\ell/2} dx \sin\left(\Phi(x,t,\boldsymbol{\alpha},\boldsymbol{\beta})\right)\right). \tag{B15}$$

By integrating out the variables a or b in this final expression, PDF's of the imaginary and real parts of $\hat{\mathcal{O}}_\ell$ can be obtained, respectively. Furthermore, the two-point function (42) immediately follows from Eq. (B8) by replacing the vector $w_j(\boldsymbol{x})$ in Eq. (B6) by $\tilde{w}_j(x) = u_j\left(\sigma e^{iq_j x} + \tau\right)$.

Appendix C: Further plots for the zero mode

We here present some additional plots for the zero mode, as governed by the quantum mechanics problem described in Sec. IV B. In particular, we show that the weak damping observed in Fig. 2 is not the only behavior found in the framework of the SCTDHA. A change in the initial conditions can cause the oscillation amplitude to increase, rather than decrease, as shown in Fig. 9. This widening of the envelope is particularly pronounced in the SCTDHA result. The exact solution soon reverts to weakly damped behaviour, though the time scale for this damping is much longer than that observed in Ref. 33. Fig. 9 presents results for $K = 1$, which corresponds to a regime in which the quadratic approximation to H_{J} (Eq. (57)) strongly deviates from the exact solution. In contrast, there is a reasonable correspondence between SCTDHA and exact results for the first few periods of oscillation. For larger values of K, this correspondence improves.

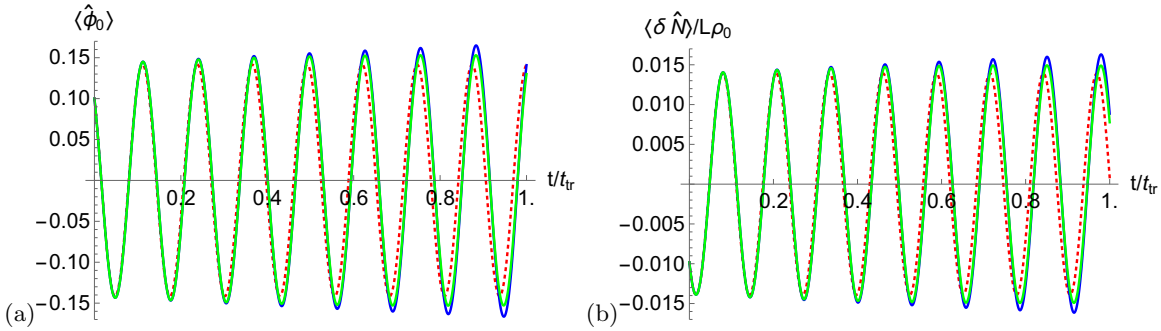

FIG. 9. Comparison between time evolution with H_{J} (green, Eq. (57)), the SCTDHA via H'_{J} (blue, Eq. (59)) and the fully quadratic Hamiltonian H_{HO} (red, Eq. (60)). Both the zero mode of the phase (a) and its conjugate variable (b) are displayed. All parameters, including the time scale, are as in Fig. 2(a), except that the sign of the initial value δN_0 is reversed.

[1] Görlitz A, Vogels J M, Leanhardt A E, Raman C, Gustavson T L, Abo-Shaeer J R, Chikkatur A P, Gupta S, Inouye S, Rosenband T and Ketterle W 2001 *Phys. Rev. Lett.* **87**(13) 130402
[2] Greiner M, Bloch I, Mandel O, Hänsch T and Esslinger T 2001 *Appl. Phys. B* **73** 769
[3] Kinoshita T, Wenger T and Weiss D S 2004 *Science* **305** 1125
[4] Rigol M, Dunjko V, Yurovsky V, and Olshanii M 2007 *Phys. Rev. Lett.* **98** 050405
[5] Calabrese P and Cardy J 2007 *J. Stat. Mech.* P06008
[6] Polkovnikov A, Sengupta K, Silva A and Vengalattore M 2011 *Rev. Mod. Phys.* **83**(3) 863
[7] Essler F H L and Fagotti M 2016 *J. Stat. Mech.* 064002
[8] Gogolin C and Eisert J 2016 *Rep. Prog. Phys.* **79** 056001
[9] Vidmar L and Rigol M 2016 *J. Stat. Mech.* 064007
[10] D'Alessio L, Kafri Y, Polkovnikov A and Rigol M 2016 *Adv. Phys.* **65** 239
[11] Calabrese P and Cardy J 2016 *J. Stat. Mech.* 064003
[12] Calabrese P 2018 *Phys. A: Stat. Mech. Appl.* **504** 31
[13] Trotzky S, Chen Y A, Flesch A, McCulloch I P, Schollwöck U, Eisert J and Bloch I 2012 *Nature Physics* **8** 325
[14] Cheneau M, Barmettler P, Poletti D, Endres M, Schauß P, Fukuhara T, Gross C, Bloch I, Kollath C and Kuhr S 2012 *Nature* **481** 484
[15] Gring M, Kuhnert M, Langen T, Kitagawa T, Rauer B, Schreitl M, Mazets I, Smith D A, Demler E and Schmiedmayer J 2012 *Science* **337** 1318
[16] Langen T, Geiger R, Kuhnert M, Rauer B and Schmiedmayer J 2013 *Nat Phys* **9** 640
[17] Langen T, Erne S, Geiger R, Rauer B, Schweigler T, Kuhnert M, Rohringer W, Mazets I E, Gasenzer T and Schmiedmayer J 2015 *Science* **348** 207
[18] Kaufman A M, Tai M E, Lukin A, Rispoli M, Schittko R, Preiss P M and Greiner M 2016 *Science* **353** 794
[19] Andrews M R, Townsend C G, Miesner H J, Durfee D S, Kurn D M and Ketterle W 1997 *Science* **275** 637
[20] Schumm T, Hofferberth S, Andersson L M, Wildermuth S, Groth S, Bar-Joseph I, Schmiedmayer J and Kruger P 2005 *Nat Phys* **1** 57
[21] Albiez M, Gati R, Fölling J, Hunsmann S, Cristiani M and Oberthaler M K 2005 *Phys. Rev. Lett.* **95**(1) 010402
[22] Gati R, Albiez M, Fölling J, Hemmerling B and Oberthaler M 2006 *Appl. Phys. B* **82** 207
[23] Levy S, Lahoud E, Shomroni I and Steinhauer J 2007 *Nature* **449** 579
[24] Hofferberth S, Lesanovsky I, Fischer B, Schumm T and Schmiedmayer J 2007 *Nature* **449** 324–327
[25] Kuhnert M, Geiger R, Langen T, Gring M, Rauer B, Kitagawa T, Demler E, Adu Smith D and Schmiedmayer J 2013 *Phys. Rev. Lett.* **110**(9) 090405

[26] Haldane F D M 1981 *Phys. Rev. Lett.* **47**(25) 1840–1843
[27] Bistritzer R and Altman E 2007 *Proc. Nat. Acad. Sci.* **104** 9955–9959
[28] Imambekov A, Gritsev V and Demler E 2007 *eprint arXiv:cond-mat/0703766* (*Preprint* cond-mat/0703766)
[29] Kitagawa T, Pielawa S, Imambekov A, Schmiedmayer J, Gritsev V and Demler E 2010 *Phys. Rev. Lett.* **104**(25) 255302
[30] Kitagawa T, Imambekov A, Schmiedmayer J and Demler E 2011 *New J. Phys.* **13** 073018
[31] Gritsev V, Polkovnikov A and Demler E 2007 *Phys. Rev. B* **75**(17) 174511
[32] Schweigler T, Kasper V, Erne S, Mazets I, Rauer B, Cataldini F, Langen T, Gasenzer T, Berges J and Schmiedmayer J 2017 *Nature* **545** 323
[33] Pigneur M, Berrada T, Bonneau M, Schumm T, Demler E and Schmiedmayer J 2018 *Phys. Rev. Lett.* **120**(17) 173601
[34] Pigneur M and Schmiedmayer J 2018 *arXiv e-prints* arXiv:1810.02772 (*Preprint* 1810.02772)
[35] Dalla Torre E G, Demler E and Polkovnikov A 2013 *Phys. Rev. Lett.* **110**(9) 090404
[36] Iucci A and Cazalilla M A 2009 *Phys. Rev. A* **80** 063619
[37] Iucci A and Cazalilla M A 2010 *New J. Phys.* **12** 055019
[38] Foini L and Giamarchi T 2015 *Phys. Rev. A* **91**(2) 023627
[39] Foini L and Giamarchi T 2017 *Eur. Phys. J. Spec. Top.* **226** 2763–2774
[40] Bertini B, Schuricht D and Essler F H L 2014 *J. Stat. Mech.* P10035
[41] Caux J S and Essler F H L 2013 *Phys. Rev. Lett.* **110**(25) 257203
[42] Caux J S 2016 *J. Stat. Mech.* 064006
[43] Calabrese P, Essler F H L and Fagotti M 2012 *J. Stat. Mech.* P07016
[44] Schuricht D and Essler F H L 2012 *J. Stat. Mech.* P04017
[45] Kormos M and Zaránd G 2016 *Phys. Rev. E* **93** 062101
[46] Sachdev S and Young A P 1997 *Phys. Rev. Lett.* **78**2220
[47] Iglói F and Rieger H 2011 *Phys. Rev. Lett.* **106**(3) 035701
[48] Cubero A C and Schuricht D 2017 *J. Stat. Mech.* 103106
[49] Horváth D and Takcs G 2017 *Phys. Lett. B* **771** 539
[50] Horváth D X, Kormos M and Takács G 2018 *J. High Energ. Phys.* 170
[51] Moca C, Kormos M and Zaránd G 2017 *Phys. Rev. Lett.* **119**(10) 100603
[52] James A J A, Konik R M, Lecheminant P, Robinson N J and Tsvelik A M 2018 *Rep. Prog. Phys.* **81** 046002
[53] Kukuljan I, Sotiriadis S and Takacs G 2018 *Phys. Rev. Lett.* **121**(11) 110402
[54] Horvath D X, Lovas I, Kormos M, Takacs G and Zarand G 2018 *ArXiv e-prints* (*Preprint* 1809.06789)
[55] Chang S J 1975 *Phys. Rev. D* **12**(4) 1071–1088
[56] Sotiriadis S and Cardy J 2010 *Phys. Rev. B* **81** 134305 (*Preprint* 1002.0167)
[57] Boyanovsky D, Cooper F, de Vega H J and Sodano P 1998 *Phys. Rev. D* **58**(2) 025007
[58] Bertini B, Essler F H L, Groha S and Robinson N J 2015 *Phys. Rev. Lett.* **115**(18) 180601
[59] Bertini B, Essler F H L, Groha S and Robinson N J 2016 *Phys. Rev. B* **94**(24) 245117
[60] van Nieuwkerk Y D and Essler F H L *In preparation*
[61] Smith D A, Gring M, Langen T, Kuhnert M, Rauer B, Geiger R, Kitagawa T, Mazets I, Demler E and Schmiedmayer J 2013 *New J. Phys.* **15** 075011
[62] Cherng R W and Demler E 2007 *New J. Phys.* **9** 7
[63] Lamacraft A and Fendley P 2008 *Phys. Rev. Lett.* **100**(16) 165706
[64] Ivanov D A and Abanov A G 2013 *Phys. Rev. E* **87**(2) 022114
[65] Shi Y and Klich I 2013 *J. Stat. Mech.* P05001
[66] Eisler V 2013 *Phys. Rev. Lett.* **111**(8) 080402
[67] Klich I 2014 *J. Stat. Mech.* P11006
[68] Stéphan J M and Pollmann F 2017 *Phys. Rev. B* **95**(3) 035119
[69] Moreno-Cardoner M, Sherson J F and De Chiara G 2016 *New J. Phys.* **18** 103015
[70] Collura M, Essler F H L and Groha S 2017 *J. Phys. A: Math. Theor.* **50** 414002
[71] Najafi K and Rajabpour M A 2017 *Phys. Rev. B* **96**(23) 235109
[72] Lovas I, Dóra B, Demler E and Zaránd G 2017 *Phys. Rev. A* **95**(5) 053621
[73] van Nieuwkerk Y D, Schmiedmayer J and Essler F H L 2018 *SciPost Phys.* **5**(5) 46
[74] Bastianello A, Piroli L and Calabrese P 2018 *Phys. Rev. Lett.* **120**(19) 190601
[75] Groha S, Essler F H L and Calabrese P 2018 *SciPost Phys.* **4** 43
[76] Bastianello A and Piroli L 2018 *J. Stat. Mech.* 113104
[77] Sakaguchi T, Tamaribuchi T and Takada S 1982 *Progr. Theor. Phys.* **68** 19
[78] Essler F H and Konik R M 2005 *Applications of Massive Integrable Quantum Field Theories to Problems in Condensed Matter Physics* (World Scientific) pp 684–830
[79] Zamolodchikov A B 1995 *Int. J. Mod. Phys. A* **10** 1125
[80] Cazalilla M A 2004 *J. Phys. B* **37** S1